Diamond & Related Materials 138 (2023) 110215

Contents lists available at ScienceDirect

Diamond & Related Materials

journal homepage: www.elsevier.com/locate/diamond

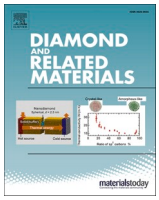

Development of semiconducting graphitic carbon nitride nanofluid for heat transfer applications: A mode mismatched thermal lens study

Vijayakumar Gokul [a], Mohanachandran Nair S. Swapna [b], Govind Ambadas [c], Sankaranarayana Iyer Sankararaman [a,*]

[a] Department of Optoelectronics, University of Kerala, Trivandrum 695581, India
[b] Laboratory for Environmental and Life Science, University of Nova Gorica, Vipavska 13, Nova Gorica SI-5000, Slovenia
[c] Department of Chemistry, University College, Trivandrum 695034, India

ARTICLE INFO

Keywords:
Graphitic carbon nitride
Hydrothermal synthesis
Portobello mushroom
Thermal lens spectroscopy

ABSTRACT

The present work delineates the heat transfer potential of the semiconducting graphitic carbon nitride (g-C_3N_4) nanofluid. The paper also discusses the eco-friendly green synthesis of g-C_3N_4 nanoparticles from the natural carbon precursor portobello mushroom by the hydrothermal method. The nanoparticles synthesised are subjected to structural, morphological, thermal, and optical characterizations. The flower-like laminar structure of the sample revealed through field emission scanning electron microscope (FESEM) analysis exhibited a semiconducting nature with an optical bandgap of 2.58 eV. The formation of g-C_3N_4 is confirmed by X-ray diffraction (XRD), Fourier transform infrared (FTIR), X-ray photoelectron (XPS) and Raman spectroscopic analyses. The thermogravimetric analysis (TGA) reveals good thermal stability up to 500 °C, which suggests possible applications in heat transfer fluids. The concentration-dependent thermal diffusivity variation of the g-C_3N_4 semiconductor nanofluid, investigated using the sensitive mode mismatched dual beam thermal lens technique, divulges its potential as an organic, metal-free additive in engine coolants for automobile applications.

1. Introduction

Semiconducting nanofluids (SNF) are a relatively new class of nanofluids consisting of nanoparticles with semiconducting properties suspended in a base fluid [1,2]. These nanoparticles, including materials like silicon, germanium, titanium dioxide (TiO_2), zinc oxide (ZnO), and cadmium sulfide (CdS), exhibit semiconducting behaviour at the nanoscale [1,3]. Semiconductor nanoparticles (SNP), as a category of nanostructured materials, possess fascinating physical, chemical, mechanical, optical, and electronic characteristics [1]. When added to a fluid, SNPs creates nanofluids with distinct properties compared to the base fluid alone [4,5]. SNF offers the advantage of manipulating the electrical and optical properties of the nanoparticles, making them highly appealing for applications in electronics and photonics [1,2]. Synthesis of SNF involves dispersing the nanoparticles within the base fluid using techniques like sonication or chemical functionalization [5–7]. The choice of base fluid varies depending on the specific application requirements, ranging from water and organic solvents to oils or polymers [4,5]. SNFs have been extensively explored for their potential in advanced cooling systems, enhancing the heat transfer capabilities of the fluid [6]. In optoelectronic applications such as solar cells and light-emitting devices, SNFs play a role in tuning the absorption or emission properties of the device [8,9]. Among the different types of SNF, organic semiconductor and their nanofluids are gaining significant attention due to their wide applications in thin-film transistors, organic light-emitting diodes, organic sensors and memory devices [1,2].

Organic semiconductors are carbon-based materials that exhibit semiconducting properties and are composed primarily of organic compounds with a conjugated π-electron system [1,8,9]. They offer unique advantages over inorganic semiconductors, including lower temperature processing, flexibility, and compatibility with large-area and low-cost manufacturing methods [8]. The properties of organic semiconductors can be customized by modifying the chemical structure, allowing for a wide range of electronic and optical properties. These materials can exhibit insulating, semiconducting, or metallic behaviour based on molecular structure and arrangement [10]. Ongoing research in the field aims to enhance the performance, stability, and understanding of organic semiconductors for applications in electronic

* Corresponding author.
E-mail address: drssraman@gmail.com (S.I. Sankararaman).

https://doi.org/10.1016/j.diamond.2023.110215
Received 11 March 2023; Received in revised form 12 June 2023; Accepted 15 July 2023
Available online 17 July 2023

devices and heat transfer.

It is significant to note that the field of SNFs is still relatively new, and ongoing research is being conducted to further explore their properties and potential applications. Like any new technology, there are difficulties to overcome, such as nanoparticle stability, aggregation, and the overall scalability of production processes. Nonetheless, SNFs hold promise for a range of applications in various industries and are an area of active research and development [11,12]. The present work delineates the potential of the semiconductor carbon nitride nanofluid for heat transfer application.

Carbon nitride refers to a class of materials composed of carbon and nitrogen atoms. The term "carbon nitride" can refer to several different compounds with varying chemical structures and properties [13]. One of the most well-known carbon nitride compounds is melamine formaldehyde polymer, which is often called melamine resin or simply melon [14]. Researchers are actively exploring different methods to synthesis carbon nitride materials with enhanced properties and investigating their potential applications in various fields. Carbon nitride-based materials have the advantage of being relatively inexpensive, abundant, and environmentally friendly, which adds to their appeal in sustainable technologies.

The CN family, one of the oldest synthetic polymers, dates back to 1834 [15,16]. In 1989, the synthesis of covalent solid CN was theoretically predicted, comparing it to diamond due to its tetrahedral sp^3 carbon structure [17,18]. Different phases of CN include α-C_3N_4, β-C_3N_4, cubic C_3N_4, quasi cubic C_3N_4, and graphitic C_3N_4 (g-C_3N_4), with g-C_3N_4 being the most stable [16,19]. g-C_3N_4 possesses a layered structure resembling graphite and exhibits enhanced stability, hardness, thermochemical tolerance, low density, wear resistance, and water imperviousness [19–21]. It is a metal-free polymeric organic semiconductor with good stability in various environments, making it popular for sustainable energy-efficient products. g-C_3N_4 nanostructures have a highly negative surface charge, enabling stable suspension in aqueous solutions [14,22]. To meet the increasing demand for CN, cost-effective and eco-friendly synthesis methods are sought, including using bio-organic products [23]. Popular synthesis methods for g-C_3N_4 include hydrothermal synthesis, solid-state reaction, electrochemical deposition, thermal decomposition, and solvothermal reaction [19,24,25].

Cost and eco-friendliness are significant concerns in the synthesis of CN. Solid-state reaction and thermal decomposition methods are expensive and environmentally unfriendly due to the need for high temperatures, high pressure, and toxic chemicals for the synthesis [19,24]. The solvothermal process requires high processing pressure, while electrochemical deposition has limitations in mass production and needs high voltage requirements. Thermal polymerization of organic precursors for CN preparation results in issues with crystallinity and limited control over nitrogen content [19,25]. A commercially viable synthesis method should consider raw material cost, energy consumption, and overall production process efficiency. Utilizing affordable and readily available precursors, optimizing reaction conditions to minimize energy requirements, and streamlining purification steps are crucial for cost-effective production [26]. Since the hydrothermal method enables the low-temperature synthesis of CN, it is widely accepted [24]. In this study, a low-temperature hydrothermal green synthesis approach using *Agaricus bisporus* — portobello mushroom as a carbon precursor is described.

g-C_3N_4 have shown great potential for various heat transfer applications due to their unique electronic and thermal properties [27]. The practical application of g-C_3N_4 as a heat transfer fluid is still at the research stage. The heat transfer property can be understood from its thermal diffusivity (D) [5,7]. Of various methods for the estimation of D, like laser-flash, temperature oscillation, transient hot wire, and photothermal (PT) method, the present work employs the laser-assisted dual beam TL technique [28]. The PT phenomena relies on the mechanism of laser-assisted excitation and non-radiative deexcitation of the molecules of the medium. The thermal energy liberated on non-radiative deexcitation induces a transient refractive index gradient resembling a lens-like element within the medium [29,30]. By suitably probing this refractive index gradient, the thermo optical properties of the medium can be studied [29]. The PT technique is highly sensitive and nondestructive as only the photon absorbed contributes to the signal. The technique is capable of sensing a temperature variation of the order of 10^{-6} °C to 10^{-4} °C, which makes it preferable to other techniques [29,30]. Among the various TL configurations like single beam, mode mismatched dual beam, and mode matched dual beam, the present study employs the sensitive mode mismatched dual beam thermal lens (MTL) technique for the thermal diffusivity study of the g-C_3N_4 nanofluid.

2. Materials and methods

Among various methods of extracting carbon templates from natural sources, the hydrothermal reaction method is a capable one with the advantages of low processing temperature, cost-effectiveness and non-toxicity [31]. As natural fibers show high specific strength and low density, it can effectively be utilized as a reinforcement material in polymer composites and an excellent source of carbon [32]. Mushrooms are widely available in nature and can be cultivated on a large scale. They are renewable sources and can be harvested without causing significant harm to the environment. This makes them a sustainable source for nitride synthesis. The present study uses *Agaricus bisporus* portobello mushroom (PM) and ammonium chloride (NH_4Cl-Sigma-Aldrich, 99.5 %) as natural carbon and nitrogen precursors, respectively, for hydrothermal synthesis of CN. PM is chosen as a carbon source because it is rich in carbohydrates (86–88 %), and other ingredients being proteins (1–2 %), crude fat (0.6–0.8 %), crude fiber (2.7–3.1 %), and ash (1–2 %) [33,34]. The PM purchased from the local market is washed in deionized water (DW) several times to remove the dirt. PM is then cut into thin slices and dried at 110 °C for 50 h in an air oven (SAKS equipment). The dried PM is powdered using an agate mortar and pestle. Hydrothermal carbonization is carried out by controlled heating of PM in the limited air supply in the air oven at 180 °C, turning the PM into a functionalized carbon precursor [35]. The proposed synthesis method is an effective physio-chemical technique that breaks long-chained carbon bonds in PM by releasing hydroxyl groups [35]. Because of the presence of the hydroxyl groups, it can undergo thermal decomposition without melting by retaining its mechanical strength [32,36]. The solution-based synthesis procedure is preferred to carry out for the uniform mixing of the precursors. The procedure ensures the incorporation of nitrogen into the carbon templates and also reduces the processing temperature [37]. The CN samples are prepared by blending the PM powder with NH_4Cl in a 1:1 ratio using DW and ethanol. 6 g of PM powder is added to 25 ml DW and kept at 45 °C with stirring at 400 rpm using a magnetic stirrer (ANTECH, AN-MSH-680) to convert it into a slurry form. 25 ml of ethanol is added to the slurry, and the stirring continues for another 30 min to enable polymer breakdown. 6 g of NH_4Cl is introduced to the solution, and the stirring continues for another 4 h at 45 °C. The solution is heated at 400 °C to release the ammonia molecules by sublimation/dissociation of NH_4Cl, which reacts with the functionalized carbon obtained after the hydrothermal reaction for the formation of C—N bonds. The heating is continued using a Bunsen burner till the solution gets dried. The resultant powder is kept in a vacuum oven (WISWO Widsons Scientific) at 200 °C for 3 h to remove the absorbed moisture. The dried powder is again grounded to enhance its surface-to-volume ratio before annealing. The grounded powder is annealed in a muffle furnace, heated up to 400 °C at the rate of 10 °C/min, and kept at that temperature for 2 h. Before further characterization, the synthesised sample is grounded using an agate mortar and pestle for half an hour to reduce its particle size. The structure characterization of the sample is carried out using Brucker d8 advanced X-ray diffractometer (Cu Kα radiation of wavelength 1.5406 Å) in the range 15°–90° at a scan speed of 0.02°/s. The surface morphology is studied using Nova nano-field emission scanning

electron microscope (FESEM). Perkin-Elmer's thermogravimetric (TG) analyser TGA-STA 6000 is used to analyse the thermal stability of the sample. The vibrational modes of the samples are analysed in the range 4000 cm^{-1}–400 cm^{-1} using Fourier transform infrared (FTIR) spectrometer (Perkin-Elmer). X-ray photoelectron spectroscopic (XPS) analysis is carried out using Thermo Fisher Scientific ESCALAB 250 Xi. Horiba Lab Ram micro-Raman spectrometer and Jasco V550 Ultraviolet–Visible (UV–Vis) spectrometer are used to record the Raman spectrum (1000 cm^{-1}–2300 cm^{-1}) and absorption spectrum (200 nm–900 nm) of the sample, respectively.

The g-C_3N_4 nanofluid is prepared by a two-step process with ethylene glycol (EG) as the base fluid. 0 mg, 0.5 mg, 1.5 mg, 2 mg, 3 mg, and 4 mg of the synthesised sample are mixed with 3 ml of EG to get different nanofluid concentrations — 0 mg·ml^{-1}, 0.17 mg·ml^{-1}, 0.50 mg·ml^{-1}, 0.67 mg·ml^{-1}, 1.00 mg·ml^{-1}, and 1.33 mg·ml^{-1}, respectively. As the literature [38] reports that stability and homogeneity of the nanofluids can be achieved through ultrasonication, the method of indirect ultrasonication using Labman LMUC-2 ultrasonicator is employed to ensure the stable dispersion of the nanoparticles in EG. The solutions are ultrasonicated for 1 h with an interval of 10 min, and the nanofluid is then subjected to TL study.

A TEM_{00} Kimmon IK series Helium-Cadmium laser (wavelength λ_e = 442 nm, power = 80 mW) and a Helium-Neon laser (wavelength λ_p = 632.8 nm, power = 2 mW) are used to set up a collinear MTL arrangement. The 442 nm and 632.8 nm lasers, respectively, act as the pump and probe beams for the MTL setup. The pump beam intensity is decreased in such a way that to obtain a blooming-free thermal lens formation inside the samples, using a neutral density filter. With the help of an electromechanical chopper (SRS-540), the pump beam is intensity modulated at 1 Hz. The pump beam is focused on the 10 mm glass cuvette (sample cell length (l)) that contains the sample, using a convex lens of a focal length of 40 cm. Using a dichroic mirror, the low intense probe is also allowed to fall at the sample center collinearly with the pump beam. The TL formation due to the probe beam is neglected, as the nanofluid shows poor absorption at the λ_p. The ratio of the square of the probe beam ($\omega_p = 1.4$ mm) and pump beam ($\omega_e = 0.236$ mm) radius at the sample center decides the degree of mode mismatching ($m = \left(\frac{\omega_p}{\omega_e}\right)^2$). The radius of the pump and probe beams are measured using Nano Scan 2S, a commercial slit beam profiler. A photodetector is used to analyse the central beam intensity variations of the probe beam. The photodetector output — TL signals are displayed in a digital storage oscilloscope (Teledyne Wavesurfer, DSO, 500 MHz). The schematic representation of the MTL setup is shown in Fig. 1.

Let I_0 be the intensity of the probe beam center at a time (t) = 0, whereas $I(t)$ is the intensity for a particular instant t. The central intensity variation can be expressed as Eq. 1 [30].

$$I(t) = I_0\left\{\left[1-\frac{\theta}{2}\,tan^{-1}\left(\frac{2mV}{\left[(1+2m)^2+V^2\right]\left(\frac{t_c}{2t}\right)+1+2m+V^2}\right)\right]^2\right\} \quad (1)$$

V is the ratio of sample cell–probe beam waist separation to the confocal distance of the probe beam. The parameter t_c is the characteristic time constant. Where θ is related to the quantities P_{th} — absorbed photothermal energy, A — absorption coefficient of the sample, and $\frac{dn}{dT}$ — refractive index gradient with respect to the temperature by the relation

$$\theta = -\frac{P_{th}Al\frac{dn}{dT}}{K\lambda_p} \quad (2)$$

The experimental TL signal is curve fitted using Eq. 1. The D of the sample can be deduced through the relation,

$$D = \frac{(\omega_e)^2}{4t_c} \quad (3)$$

The information regarding the amount of heat absorbed and the extent of the heated region during the laser-matter interaction can be revealed by observing the nanofluid's change in refractive index (Δn). MATLAB software is used to simulate Δn variations (Eq. 4) at a point 'r' and at a time 't'.

$$\Delta n = n(r,t) - n_0 = \frac{dn}{dT}\Delta T(r,t) = \frac{\theta\lambda_e}{2\pi l t_c}\int_0^t \frac{1}{1+\frac{2t'}{t_c}} e^{\left(\begin{array}{c}\frac{2r^2}{\omega_e^2} \\ -\frac{\omega_e^2}{1+\frac{2t'}{t_c}}\end{array}\right)} dt' \quad (4)$$

3. Result and discussions

The synthesised sample's structure, morphology and other physical properties are analysed using different characterization techniques. The X-ray diffraction analysis gives an idea regarding a material's crystallographic structure, size, phase, and chemical composition. Fig. 2a shows the XRD pattern of the synthesised sample. The diffraction peaks 27.8°, 32.4°, 40.1°, 46.6°, 49.3°, 58.1°, 73.3°, 77.8°, and 87° correspond to the (110), (200), (101), (111), (300), (211), (320), (002), and (202)

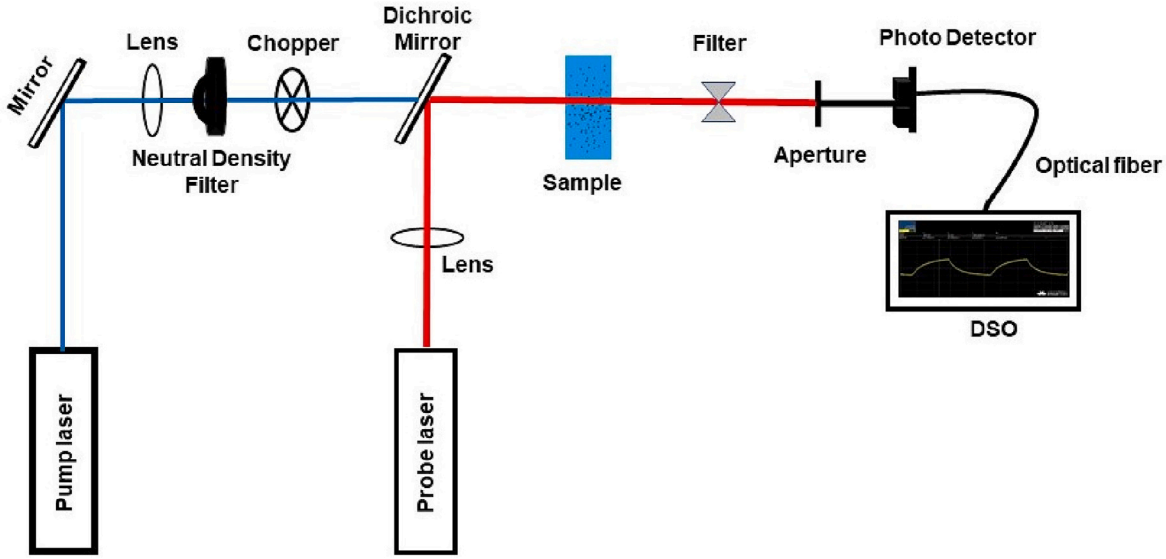

Fig. 1. Schematic of the mode mismatched dual beam thermal lens setup.

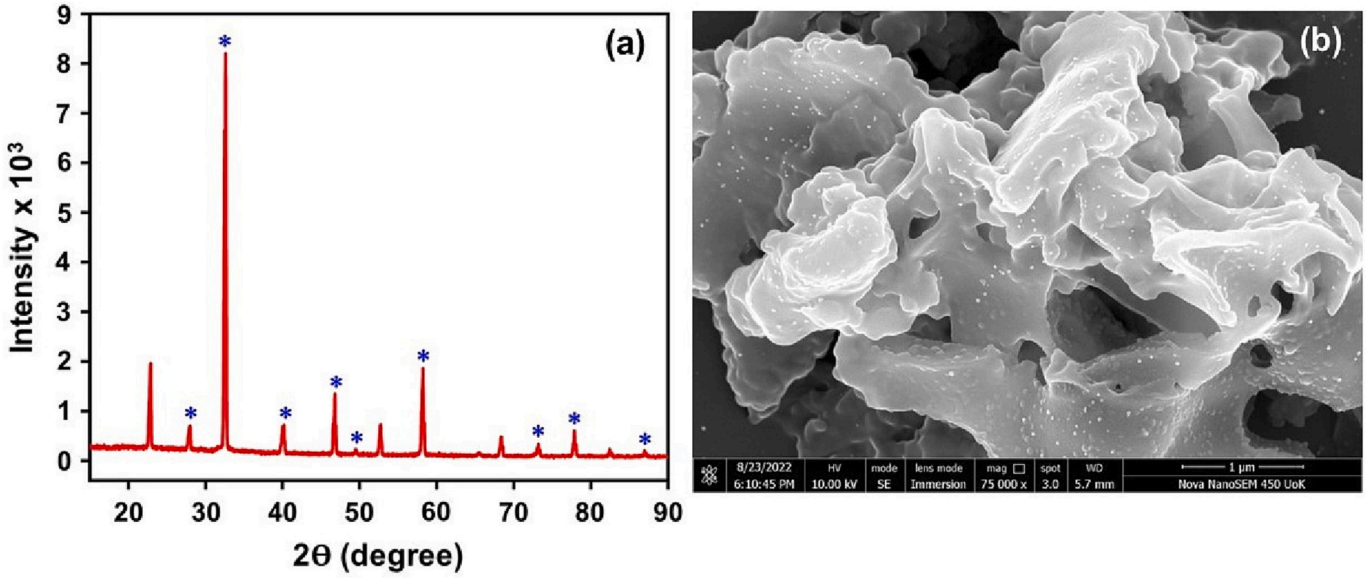

Fig. 2. (a) XRD pattern, (b) FESEM image of the synthesised sample.

planes indexed to hexagonal g-C_3N_4 (ICDD file — 00-050-1250). The appearance of the peak at 27.8° is a result of the stacking of conjugated aromatic systems. This is generally attributed to graphitic materials. Thus the formation of g-C_3N_4 is evident from the diffraction spectrum [39]. The formation of the excellent crystalline peaks of the hydrothermally synthesised g-C_3N_4 sample reveals the reliability of the synthesis route adopted in the study. The preparation of g-C_3N_4 by X. Li et al. [40] and J. Yang et al. [41] through pyrolysis of melamine at 800 °C and 1000 °C respectively, and C. Fan et al. [42] by direct heating observed only a strongest XRD peak at 27.8°. The lattice parameter of the synthesised g-C_3N_4 is obtained as a = b = 6.42 Å, c = 2.46 Å. The lattice parameters and the peak position agree with the values in the ICDD files of g-C_3N_4. The sample's average crystallite size (τ) is calculated using the Scherrer equation [43] and obtained as 29.83 nm. The thermophysical properties of the synthesised material get influenced by the dislocations that arise within. These defects in a crystalline structure can be revealed by calculating the dislocation density (δ), which represents the dislocation length per unit volume. Eq. 5 is used to calculate the dislocation density [44]

$$\delta = \frac{15\beta\cos(\theta)}{4a\tau} \tag{5}$$

where β is the full-width half maximum (FWHM), θ is Braggs' diffraction angle, and a is the lattice constant. The δ is obtained as 1.126×10^{-3} nm^{-2}. The number of unit cells (N) per unit volume is calculated as 157,892 using Eq. 6 [44]

$$N = \frac{4\pi\left(\frac{\tau}{2}\right)^3}{3V} \tag{6}$$

where V is the cell volume of the sample. The dislocation density is inversely proportional to crystallite size and the number of unit cells. The morphology of the sample is also understood from the morphology index (M) calculated from the XRD spectrum using Eq. 7. Let β_h be the highest FWHM values obtained from the XRD peaks, and β_p be the value of a specific XRD peak for which M is to be calculated [44]. To analyse the parameter M, the peak at 32.4° is taken as β_p, and the value of M is obtained as 0.559.

$$M = \frac{\beta_h}{\beta_h + \beta_p} \tag{7}$$

The morphology of the sample, as revealed from the FESEM images shown in Fig. 2b, is found to be a flower-like laminar structure. The hydrothermal treatment leads to the softening of the g-C_3N_4 flower-like porous sheets and also modifies the surface chemical functionalities [26,45]. For heat transfer applications thermal stability of the NP is highly significant, which is understood from the TG analysis carried out in a nitrogen atmosphere from 30 °C to 800 °C. Fig. 3a shows the TGA of the synthesised sample. Compared to the literature [40,41] the synthesised sample shows good thermal stability with a weight loss of less than 20 % up to 500 °C.

The peaks that appear in the FTIR spectrum give information regarding the structure, vibrational modes, and functional groups present inside the synthesised sample [37]. Fig. 3b shows the FTIR spectrum of the synthesised sample recorded in the range of 4000 cm^{-1} to 400 cm^{-1}. The O—H vibrations of absorbed water on the surfaces and the stretching and deformation modes of the NH_2 groups can be observed in the region 3426 cm^{-1} to 3025 cm^{-1}. The region between 3125 cm^{-1} to 2805 cm^{-1} originates from the uncondensed terminal amino groups' (–NH, ═NH) vibrational modes [39] and the skeletal C═N heterocycle stretches, containing trigonal (N—C_3) and C—NH—C bridging units C—N—C network. The small peak at 2019 cm^{-1} is due to the C≡N (nitrile) group and similar species. This indicates the presence of some C≡N in the sample [41]. The indication of g-C_3N_4 structure formation is attributed to the peaks 1738 cm^{-1} to 1396 cm^{-1} region. The peak at 1396 cm^{-1} is due to the stretching vibrations of the *s*-triazine ring units [42]. The hydrothermally green synthesised sample shows a strong triazine ring peak, which clearly confirms the formation of g-C_3N_4. But the g-C_3N_4 prepared through thermal pyrolysis lacks the dominance of this peak [40]. The peak at 1630 cm^{-1} is of C═N vibrational modes, and at 1540 cm^{-1} and 1080 cm^{-1} correspond to aromatic C—N stretching mode. The stretching vibrations NH_2 groups associated with the carbon nanobelts appeared to peak at 614 cm^{-1} [41]. The FTIR analysis thus confirms the formation of g-C_3N_4 in the synthesised sample.

The nature of chemical bonding, oxidation states, elemental composition and the functional groups present in a sample is understood from the surface-sensitive XPS analysis technique. The XPS survey spectrum (Fig. 4a) confirms the presence of carbon, nitrogen, and oxygen in the synthesised sample. The deconvoluted high-resolution XPS spectra of C1s, N1s, and O1s are shown in Fig. 4b, c, and d, respectively. The peak at 286.5 eV corresponds to the sp^2-bonded carbon in C—N bonds [46]. The peaks at 293.4 eV and 283.9 eV reveal the presence of sp^2-bonded C—C and π–π* transitions, respectively [47]. The 283.9 eV peak is also assigned to the formation of graphitic states in the C—N

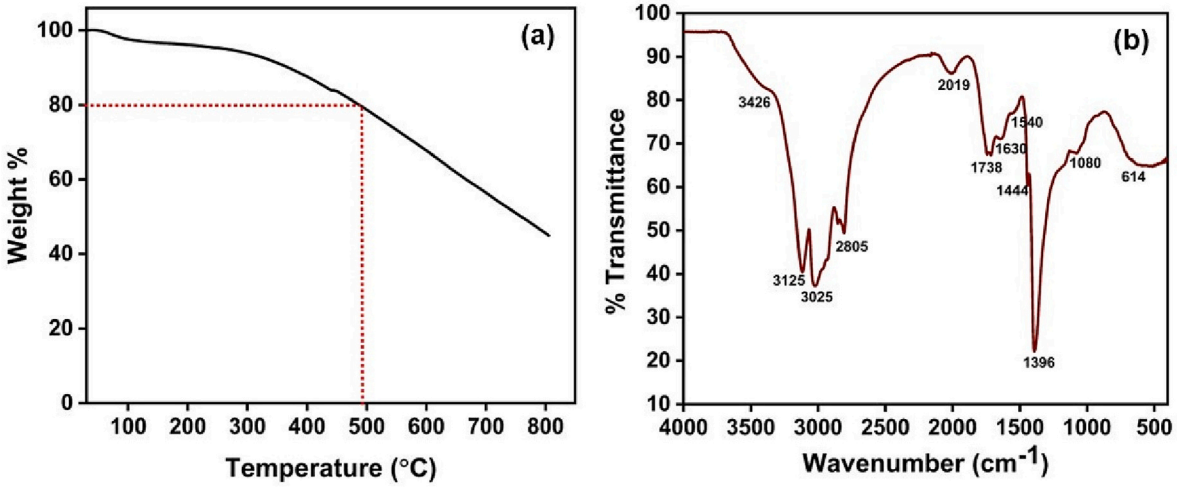

Fig. 3. (a) TGA plot, (b) FTIR spectrum of the synthesised sample.

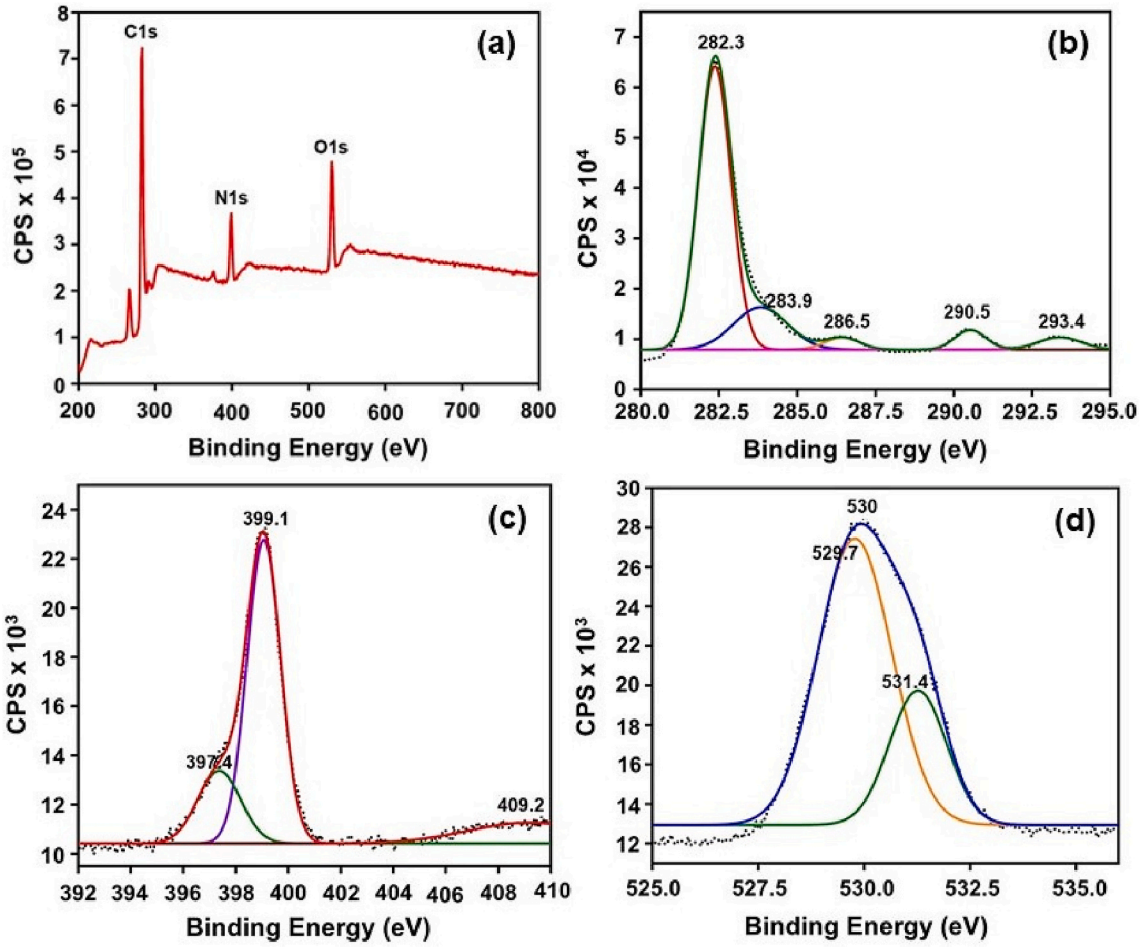

Fig. 4. (a) XPS survey spectrum of the synthesised sample. The deconvoluted peaks of (b) C1s core levels, (c) N1s core level, (d) O1s core level (dotted and solid lines represent the original and the deconvoluted curves, respectively).

matrix. The 286.5 eV peak is of the rise of –C≡N (nitrile) functional groups [48]. A peak at 290.5 eV (C═O) proposes surface degradation due to the oxygen-containing functional groups in the synthesised sample [49]. The N1s core signal of g-C_3N_4 at 399.1 eV and 397.4 eV is due to the bridging sp^3 bonded N—C_3 and sp^2 bonded C═N—C in triazine ring groups, respectively, which is the important aromatic carbon species in the polymeric g-C_3N_4 [42,46]. The peaks at 530 eV upon deconvolution discloses the N—C═O at 529.7 eV and absorbed moisture at 531.3 eV [49]. Thus, the XPS analysis confirms the formation of g-C_3N_4 in the synthesised sample, which agrees well with the XRD and FTIR analyses.

For affirming the structure and nature of bonding in the sample, the

Raman spectrum of the sample is recorded and is shown in Fig. 5a. The disordered peak (D band) of the A_{1g} mode arises at 1328 cm^{-1} due to the in-plane vibration of all sp^2 bonded carbons, originating due to the graphitic structural distortions caused by grain boundaries of N and sp^3 bonded carbons. The graphitic peak (G band) 1570 cm^{-1} corresponds to the symmetric E_{2g} vibrational modes observed in graphite-like materials. The 2196 cm^{-1} peak is contributed by the C≡N stretching vibrations [46,50]. The relative intensity of the D and G bands ($\frac{I_D}{I_G}$) is 1.05, showing the measure of disorder within the synthesised sample structure. The semiconducting nature of the sample is understood by estimating the optical bandgap from the UV–Vis absorption spectrum. UV–Vis absorption spectrum and its Tauc plot of the synthesised sample are displayed in Fig. 5b and c, respectively. The absorption bump at 306 nm and 370 nm are due to the π–π* overlapped electron transition in sp^2 hybridised conjugated aromatic g-C_3N_4 and n–π* electron lone pairs due to N-defect sites such as N vacancies and –C≡N heptazine groups respectively [25,48]. From the Tauc plot, the bandgap for the synthesised sample is determined as 2.58 eV, which reveals the semiconducting nature of the synthesised g-C_3N_4.

The potentiality of the synthesised semiconducting g-C_3N_4 as a heat transfer fluid can be analysed by finding the thermal diffusivity of the nanofluid. The synthesised g-C_3N_4 is mixed in the base fluid EG at different concentrations to study the concentration-dependent D variation. A highly sensitive, non-contact, non-destructive MTL technique is employed for the analysis. MTL setup is initially standardised by finding the base fluid's D ($(0.93 \pm 0.02) \times 10^{-7}$ $m^2 \cdot s^{-1}$) [37]. Eq. 4 is used to calculate the temperature dependant refractive index change happening inside the nanofluids. Fig. 6 shows the Δn variation for the different concentrations of g-C_3N_4 in the base fluid EG. The blooming pattern induced by the intensity-modulated pump beam inside the sample is shown in Fig. 7a. This confirms the formation of TL within the sample. The periodic deposition of heat to the medium as a result of non-radiative relaxation induces a temperature gradient inside the medium. This leads to the formation of thermal blooming [51]. The deposition of heat inside the medium produces a lensing effect which can be convex or concave in nature, depending on the type of refractive index gradient of the medium. The propagation of the thermal wave developed due to the periodic laser-medium interaction depends on the t_c. The rings observed in Fig. 7a are due to the thermal wave propagation through the medium [51]. A neutral density filter is used to minimize this aberration before recording the TL signal. Fig. 7b and c represent the decay signal for the base fluid and nanofluid for the concentration of 1.33 $mg \cdot ml^{-1}$, respectively. The θ and t_c values can be deduced by curve fitting the obtained signals using Eq. 1, and D can be calculated using Eq. 3. Fig. 8a shows the thermal diffusivity variation with respect to different concentrations of the nanofluid. From this, it is evident that the D of the nanofluid enhances with the increase in the concentration of g-C_3N_4. When the concentration of the nanoparticles in the base fluid increases, rapid energy transfer happens through electron-phonon interaction [52] and also, the effective heat propagation path through the solid increases [53]. The increase in concentration improves the optical absorption, leading to more thermal energy deposition in the medium. It is clear from Eq. 2 that the parameter θ is a measure of the thermal energy deposited in the medium due to pump beam irradiation. The increase of $|\theta|$ with g-C_3N_4 concentration, as shown in Fig. 8b, indicates the deposition of heat energy in the sample. This justifies the increase in the D value with respect to the increase in the nanofluid concentration without sedimentation, which is understood from the ageing studies using the UV–Vis absorption spectrum. Thermal diffusivity indicates how fast a material medium can propagate heat energy [54]. The study reveals that adding g-C_3N_4 nanoparticles to the base fluid significantly enhances the nanofluid's thermal diffusivity. The enhancement in D enables more effective heat transfer in green synthesised organic semiconducting g-C_3N_4 NF, making it suitable for applications in heat exchangers, cooling systems and thermal management of electronic devices.

4. Conclusion

Semiconducting nanofluids are a nascent field, and continuous investigations are underway to delve deeper into their characteristics and potential uses. Like any budding technology, there are obstacles to surmount, including maintaining nanoparticle stability, preventing aggregation, and achieving scalable production methods. Nevertheless, semiconducting nanofluids exhibit great potential for diverse industries and remain an actively explored domain of research and development. The present work delineates the low-temperature green synthesis of the semiconducting g-C_3N_4 by hydrothermal method using portobello mushroom as the natural carbon precursor. The structure of the sample revealed from the XRD analysis and the bondage between carbon and nitrogen from FTIR, XPS, and Raman analyses confirm the formation of g-C_3N_4. The TGA indicates excellent thermal stability of the synthesised sample. The UV–Vis spectroscopic analysis of the sample reveals the optical bandgap energy as 2.58 eV indicating its semiconducting nature. The possibility of the semiconducting g-C_3N_4 in the emerging area of heat transfer nanofluid has been investigated using a highly sensitive mode mismatched dual-beam thermal lens technique. For studying the thermal exchange behaviour, nanofluid is prepared with the base fluid, ethylene glycol and the concentration-dependent thermal diffusivity (D) of g-C_3N_4 nanofluid is investigated. The study reveals that the value of D increases with increasing concentration indicating the enhancement in heat conduction with concentration. Thus, the paper delineates the low-temperature, and low-cost green synthesised g-C_3N_4 using a natural carbon precursor — portobello mushroom for heat transfer applications.

Funding

This research did not receive any specific grant from funding agencies in the public, commercial, or not-for-profit sectors.

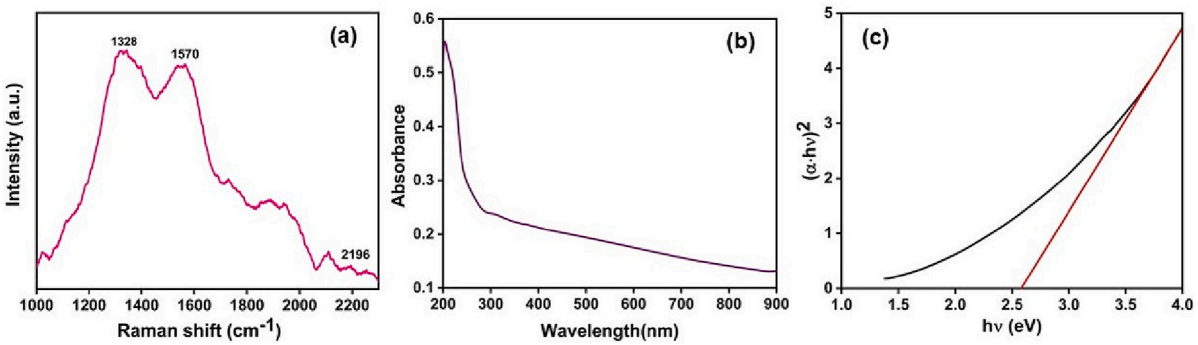

Fig. 5. (a) Raman spectrum, (b) UV–Vis spectrum, (c) Tauc plot of the synthesised sample.

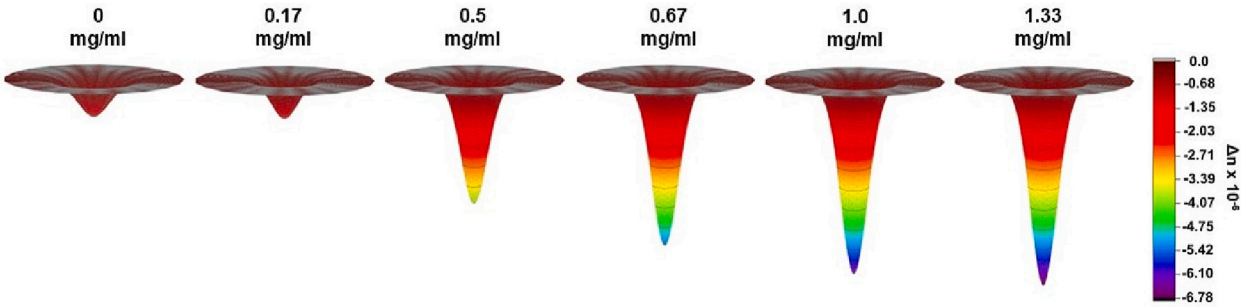

Fig. 6. Refractive index profile of the different nanofluids.

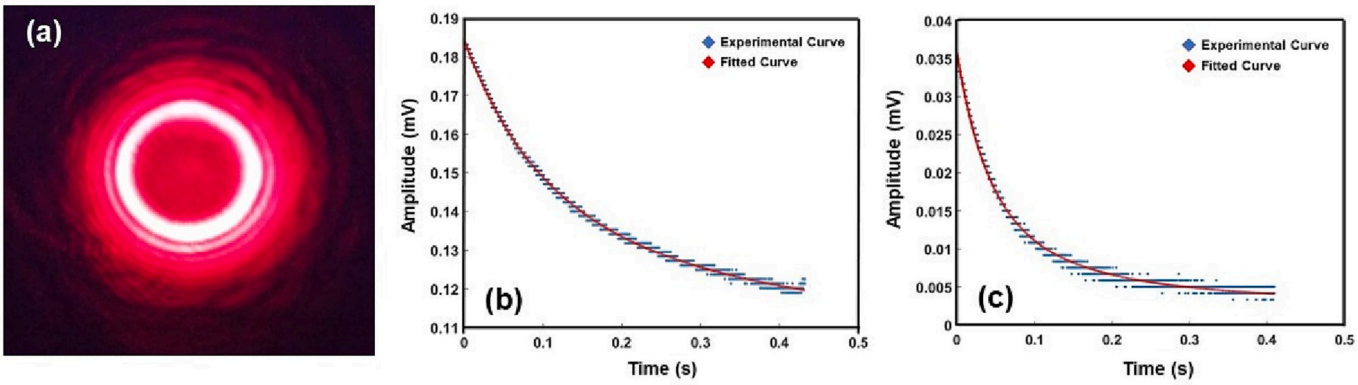

Fig. 7. (a) Thermal blooming. Thermal decay signal of (b) base fluid, (c) g-C_3N_4 nanofluid for concentration = 1.33 mg·ml^{-1}.

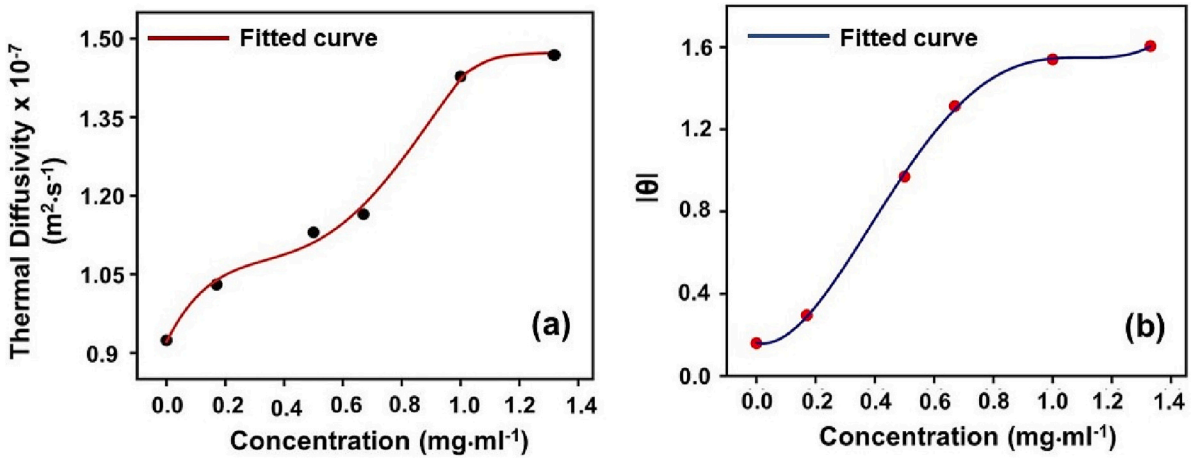

Fig. 8. (a) Variation of the thermal diffusivity of the nanofluid for different concentrations of g-C_3N_4 with respect to base fluid, (b) variation of parameter θ with respect to concentration.

CRediT authorship contribution statement

Vijayakumar Gokul: Methodology, Software, Formal analysis, Writing – original draft. **Mohanachandran Nair S. Swapna:** Validation, Formal analysis, Writing – review & editing. **Govind Ambadas:** Writing – review & editing, Supervision. **Sankaranarayana Iyer Sankararaman:** Validation, Formal analysis, Writing – review & editing, Supervision.

Declaration of competing interest

The authors declare that they have no known competing financial interests or personal relationships that could have appeared to influence the work reported in this paper.

Data availability

No data was used for the research described in the article.

Acknowledgement

Acknowledging Central Laboratory for Instrumentation and Facilitation (CLIF), University of Kerala, Trivandrum, 695581, India, for providing an instrumentation facility. The authors are thankful to B. S. Sreelekshmi, postgraduate student, Department of Chemistry, University College, Trivandrum, 695034, India, for her help during the

research work.

References

[1] A.D. Terna, E.E. Elemike, J.I. Mbonu, O.E. Osafile, R.O. Ezeani, The future of semiconductors nanoparticles: synthesis, properties and applications, Mater. Sci. Eng. B 272 (2021), 115363, https://doi.org/10.1016/j.mseb.2021.115363.

[2] V.I. Klimov, Semiconductor and Metal Nanocrystals: Synthesis and Electronic and Optical Propeties, Marcel Dekker, New York, USA, 2004, pp. 83–304.

[3] D.M.P. Mingos, X. Peng, Semiconductor Nanocrystals and Silicate Nanoparticles, Springer, Heidelberg, 2005.

[4] J.L. Jiménez-Pérez, J.F. Sánchez-Ramírez, D. Cornejo-Monroy, R. Gutierrez-Fuentes, J.A. Pescador Rojas, A. Cruz-Orea, M.A. Algatti, C. Jacinto, Photothermal study of two different nanofluids containing SiO_2 and TiO_2 semiconductor nanoparticles, Int. J. Thermophys. 33 (2012) 69–79, https://doi.org/10.1007/s10765-011-1139-z.

[5] S.U.S. Choi, J.A. Eastman, Enhancing thermal conductivity of fluids with nanoparticles, Am. Soc. Mech. Eng. Fluids Eng. Div. 231 (1995) 99–105. https://www.osti.gov/servlets/purl/196525.

[6] S.P. Singh, A.K. Verma, A.K. Jaiswal, D. Singh, R.R. Yadav, Study of ultrasonic and thermal properties for heat transfer enhancement in Fe_2O_3 nanoparticles-ethylene glycol nanofluids, Int. J. Thermophys. 42 (2021) 1–17, https://doi.org/10.1007/s10765-021-02809-w.

[7] S.K. Das, S.U.S. Choi, W. Yu, T. Pradeep, Nanofluids: Science and Technology, John Wiley & Sons, United States of America, 2005.

[8] W. Brütting, Physics of Organic Semiconductors, Wiley-VCH, Weinheim, 2006, https://doi.org/10.1002/3527606637.

[9] S. Atahan-Evrenk, A. Aspuru-Guzik, Prediction and theoretical characterization of p-type organic semiconductor crystals for field-effect transistor applications, Top. Curr. Chem. 345 (2014) 95–138, https://doi.org/10.1007/128_2013_526.

[10] S. Suresh, Semiconductor nanomaterials, methods and applications: a review, Nanosci. Nanotechnol. 3 (2013) 62–74, https://doi.org/10.5923/j.nn.20130303.06.

[11] K. Rani, Nano semiconductors: a study on its importance and uses, J. Adv. Sch. Res. Allied Edu. 12 (2017) 1536–1540, https://doi.org/10.29070/JASRAE.

[12] M.M.R. Sha, S. Mathew, S. Udayan, V.P.N. Nampoori, A. Mujeeb, Ultra-pure silicon nanofluid by laser ablation: thermal diffusivity studies using thermal lens technique, Appl. Phys. B Lasers Opt. 124 (2018) 1–7, https://doi.org/10.1007/s00340-018-7081-z.

[13] A. Alaghmandfard, K. Ghandi, A comprehensive review of graphitic carbon nitride ($g\text{-}C_3N_4$)–metal oxide-based nanocomposites: potential for photocatalysis and sensing, Nanomater. 12 (2022) 1–73, https://doi.org/10.3390/nano12020294.

[14] J. Liu, H. Wang, M. Antonietti, Graphitic carbon nitride "reloaded": emerging applications beyond (photo)catalysis, Chem. Soc. Rev. 45 (2016) 2308–2326, https://doi.org/10.1039/c5cs00767d.

[15] J.J. Liebig, Uber einige Stickstoff-Verbindungen, Ann. Phar. 10 (1834) 1–47, https://doi.org/10.1002/jlac.18340100102.

[16] Z. Zhou, Y. Zhang, Y. Shen, S. Liu, Y. Zhang, Molecular engineering of polymeric carbon nitride: advancing applications from photocatalysis to biosensing and more, Chem. Soc. Rev. 47 (2018) 2298–2321, https://doi.org/10.1039/c7cs00840f.

[17] A.Y. Liu, M.L. Cohen, Prediction of new low compressibility solids, Science. 245 (1989) 841–842, https://doi.org/10.1126/science.245.4920.841.

[18] D.C. Nesting, J.V. Badding, High pressure synthesis of sp^2 bonded carbon nitrides, Chem. Mater. 8 (1996) 1535–1539, https://doi.org/10.1021/Cm9601289, 0.357.

[19] Q. Hao, G. Jia, W. Wei, A. Vinu, Y. Wang, H. Arandiyan, B.J. Ni, Graphitic carbon nitride with different dimensionalities for energy and environmental applications, Nano Res. 13 (2020) 18–37, https://doi.org/10.1007/s12274-019-2589-z.

[20] C. Cheng, J. Shi, L. Mao, C. Dong, Y. Huang, S. Zong, Ultrathin porous graphitic carbon nitride from recrystallized precursor toward significantly enhanced photocatalytic water splitting, J. Colloid Interface Sci. 637 (2023) 271–282, https://doi.org/10.1016/j.jcis.2023.01.098.

[21] G. Dong, Y. Zhang, Q. Pan, J. Qiu, A fantastic graphitic carbon nitride ($g\text{-}C_3N_4$) material: electronic structure, photocatalytic and photoelectronic properties, J Photochem Photobiol C: Photochem Rev 20 (2014) 33–50, https://doi.org/10.1016/j.jphotochemrev.2014.04.002.

[22] C. Cheng, L. Mao, X. Kang, C. Dong, Y. Huang, S. Shen, J. Shi, L. Guo, A high-cyano groups content amorphous crystalline carbon nitride isotype heterojunction photocatalyst for high quantum yield H_2 production and enhanced CO_2 reduction, Appl. Catal. B. 331 (2023), 122733, https://doi.org/10.1016/j.apcatb.2023.122733.

[23] H.C. Yang, M.W. Chao, C.J. Chou, K.H. Wang, C. Hu, Mushroom waste-derived $g\text{-}C_3N_4$ for methyl blue adsorption and cytotoxic test for Chinese hamster ovary cells, Mater. Chem. Phys. 244 (2020), 122715, https://doi.org/10.1016/j.matchemphys.2020.122715.

[24] P. Zhang, X. Li, C. Shao, Y. Liu, Hydrothermal synthesis of carbon-rich graphitic carbon nitride nanosheets for photoredox catalysis, J. Mater. Chem. A 3 (2015) 3281–3284, https://doi.org/10.1039/c5ta00202h.

[25] J. Bian, C. Huang, R.Q. Zhang, Graphitic carbon nitride film: an emerging star for catalytic and optoelectronic applications, ChemSusChem. 9 (2016) 1–14, https://doi.org/10.1002/cssc.201600863.

[26] H.V. Sarithadevi, M.S. Swapna, V. Raj, G. Ambadas, S. Sankararaman, Natural cotton as precursor for the refractory boron carbide — a hydrothermal synthesis and characterization, Mater. Res. Express. 5 (2018) 15603, https://doi.org/10.1088/2053-1591/aaa367.

[27] Y. Ma, Y. Yang, C. Lu, K. Lu, S. Wu, X. Liu, X. Wen, Comparison of graphene oxide and graphitic carbon nitride filled carbon-phenolic composites: thermomechanical properties and role of the strong electronegativity of nanofillers, J. Appl. Poly. Sci. 46242 (2018) 1–12, https://doi.org/10.1002/app.46242.

[28] M.S. Swapna, V. Raj, H. Cabrera, S. Sankararaman, Thermal lensing of multi-walled carbon nanotube solutions as heat transfer nanofluids, ACS Appl. Nano Mater. 4 (2021) 3416–3425, https://doi.org/10.1021/acsanm.0c03219.

[29] M. Franko, C.D. Tran, Analytical thermal lens instrumentation, Rev. Sci. Inst. 67 (1996) 1–18, https://doi.org/10.1063/1.1147512.

[30] J. Shen, R.D. Lowe, R.D. Snook, A model for cw laser induced mode-mismatched dual-beam thermal lens spectrometry, Chem. Phys. 165 (1992) 385–396, https://doi.org/10.1016/0301-0104(92)87053-C.

[31] H.V. Sarithadevi, M.S. Swapna, G. Ambadas, S. Sankararaman, Optical emission diagnosis of boron carbide synthesized using natural carbon precursors, Opt. Spectrosc. 125 (2018) 928–932, https://doi.org/10.1134/S0030400X18120251.

[32] M.S. Swapna, H.V. Sarithadevi, R. Sebastian, G. Ambadas, S. Sankararaman, Natural precursor based hydrothermal synthesis of sodium carbide for reactor applications, Mater. Res. Express. 4 (2017), 125602, https://doi.org/10.1088/2053-1591/aa9db9.

[33] R.C.G. Corrêa, T. Brugnari, A. Bracht, R.M. Peralta, I.C.F.R. Ferreira, Biotechnological, nutritional and therapeutic uses of *Pleurotus* spp. (oyster mushroom) related with its chemical composition: a review on the past decade findings, Trends Food Sci. Technol. 50 (2016) 103–117, https://doi.org/10.1016/j.tifs.2016.01.012.

[34] P. Kalač, A review of chemical composition and nutritional value of wild-growing and cultivated mushrooms, J. Sci. Food Agric. 93 (2013) 209–218, https://doi.org/10.1002/jsfa.5960.

[35] H.V. Sarithadevi, M.S. Swapna, G. Ambadas, S. Sankararaman, Low-temperature green synthesis of boron carbide using aloe vera, Chin. Phys. B 27 (2018), 065303, https://doi.org/10.1088/1674-1056/27/10/107702.

[36] H.V. Sarithadevi, M.S. Swapna, G. Ambadas, S. Sankararaman, Hydrothermal development and characterization of the wear-resistant boron carbide from Pandanus: a natural carbon precursor, Appl. Phys. A Mater. Sci. Proces. 124 (2018) 1–7, https://doi.org/10.1007/s00339-018-1733-z.

[37] V. Gokul, M.S. Swapna, V. Raj, H.V. Sarithadevi, S. Sankararaman, Concentration-dependent thermal duality of hafnium carbide nanofluid for heat transfer applications: a mode mismatched thermal lens study, Int. J. Thermophys. 42 (2021) 1–12, https://doi.org/10.1007/s10765-021-02859-0.

[38] A. Afzal, I. Nawfal, I.M. Mahbubul, S.S. Kumbar, An overview on the effect of ultrasonication duration on different properties of nanofluids, J. Therm. Anal. Calorim. 135 (2018) 393–418, https://doi.org/10.1007/s10973-018-7144-8.

[39] H. Li, Y. Jing, X. Ma, T. Liu, L. Yang, B. Liu, S. Yin, Y. Wei, Y. Wang, Construction of a well-dispersed Ag/graphene like $g\text{-}C_3N_4$ photocatalyst and enhanced visible light photocatalytic activity, RSC Adv. 7 (2017) 8688–8693, https://doi.org/10.1039/c6ra26498k.

[40] X. Li, J. Zhang, L. Shen, Y. Ma, W. Lei, Q. Cui, G. Zou, Preparation and characterization of graphitic carbon nitride through pyrolysis of melamine, Appl. Phys. A Mater. Sci. Process. 94 (2009) 387–392, https://doi.org/10.1007/s00339-008-4816-4.

[41] J. Yang, X. Wu, X. Li, Y. Liu, M. Gao, X. Liu, L. Kong, S. Yang, Synthesis and characterization of nitrogen-rich carbon nitride nanobelts by pyrolysis of melamine, Appl. Phys. A Mater. Sci. Process. 105 (2011) 161–166, https://doi.org/10.1007/s00339-011-6471-4.

[42] C. Fan, J. Miao, G. Xu, J. Liu, J. Lv, Y. Wu, Graphitic carbon nitride nanosheets obtained by liquid stripping as efficient photocatalysts under visible light, RSC Adv. 7 (2017) 37185–37193, https://doi.org/10.1039/c7ra05732f.

[43] A.L. Patterson, The scherrer formula for X-ray particle size determination, Phys. Rev. 56 (1939) 978–982, https://doi.org/10.1103/PhysRev.56.978.

[44] R.H.P. Devamani, M. Alagar, Synthesis and characterisation of copper II hydroxide nano particles, Nano Biomed. Eng. 5 (2013) 116–120, https://doi.org/10.5101/nbe.v5i3.p116-120.

[45] O. Stroyuk, O. Raievska, D.R.T. Zahn, Graphitic carbon nitride nanotubes: anew material for emerging applications, RSC Adv. 10 (2020) 34059–34087, https://doi.org/10.1039/d0ra05580h.

[46] P. Petrov, D.B. Dimitrov, D. Papadimitriou, G. Beshkov, V. Krastev, C. Georgiev, Raman and X-ray photoelectron spectroscopy study of carbon nitride thin films, Appl. Surf. Sci. 151 (1999) 233–238, https://doi.org/10.1016/S0169-4332(99)00278-0.

[47] N. Urakami, M. Kosaka, Y. Hashimoto, Thermal chemical vapor deposition and luminescence property of graphitic carbon nitride film for carbon-based semiconductor systems, Jpn. J. Appl. Phys. 58 (2019) 10907, https://doi.org/10.7567/1347-4065/aaf225.

[48] W. Wang, H. Zhang, S. Zhang, Y. Liu, G. Wang, C. Sun, H. Zhao, Potassium ion assisted regeneration of active cyano groups in carbon nitride nanoribbons: visible-light driven photocatalytic nitrogen reduction, Angew. Chem. Int. Ed. 58 (2019) 16644–16650, https://doi.org/10.1002/anie.201908640.

[49] T.V. de Medeiros, A.O. Porto, H.A. Bicalho, J.C. González, R. Naccache, A.P. C. Teixeira, The effects of chemical and thermal exfoliation on the physico-chemical and optical properties of carbon nitrides, J. Mater. Chem. C 9 (2021) 7622–7631, https://doi.org/10.1039/d1tc01734a.

[50] I. Widlow, Y.W. Chung, Synthesis and characterisation of carbon nitride thin films, Int. Mater. Rev. 47 (2002) 153–167, https://doi.org/10.1179/095066002225005206.

[51] R. Sebastian, M.S. Swapna, V. Raj, M. Hari, S. Sankararaman, Thermal diffusivity control in titanium dioxide nanofluid through phase tuning, Mater. Res. Express. 5 (2018), 075001, https://doi.org/10.1088/2053-1591/aab41d.

[52] B. Rajesh Kumar, N. Shemeena Basheer, S. Jacob, A. Kurian, S.D. George, Thermal-lens probing of the enhanced thermal diffusivity of gold nanofluid-ethylene glycol mixture, J. Therm. Anal. Calorim. 119 (2015) 453–460, https://doi.org/10.1007/s10973-014-4208-2.

[53] M.S. Swapna, S. Sankararaman, Generalized theory of thermal conductivity for different media: solids to nanofluids, J. Phys. Chem. C 123 (2019) 23264–23271, https://doi.org/10.1021/acs.jpcc.9b07406.

[54] V. Gokul, M.S. Swapna, V. Raj, S.V. Gratowski, S. Sankararaman, Development of zinc oxide-multi-walled carbon nanotube hybrid nanofluid for energy-efficient heat transfer application: a thermal lens study, Phys. Fluids 33 (2021), 107108, https://doi.org/10.1063/5.0067041.